JOURNAL OF APPLIED ELECTROCHEMISTRY 23 (1993) 1214–1222

Modelling of the sodium-ferrous chloride electrochemical cell

S. W. ORCHARD*, J. S. WEAVING

Department of Chemistry, University of the Witwatersrand, Private Bag 3, Wits 2050, South Africa

Received 20 October 1992

A computer model of the discharge behaviour of the Na–$FeCl_2$ cells is presented. The cell comprises a liquid sodium anode and a porous iron/iron chloride cathode impregnated with NaCl-saturated $AlCl_3$: NaCl molten electrolyte. The anode and cathode are separated by a β''-alumina solid electrolyte. Both cylindrical (inner and outer cathodes) and flat-plate cell geometries can be simulated. Macroscopic porous electrode theory is used. The cathode reaction is considered to be effectively a solid state process, in that the solubilities of $FeCl_2$ and NaCl are not taken into account. The model predictions show good correspondence with experimental data. The results provide useful insight into cell performance in general and the detailed performance of the cathode in particular.

List of symbols

A	area (cm^2)
b	tortuosity factor (= 1.5)
D	depth of discharge of cathode (overall)
d	depth of discharge of cathode (segment)
ΔE	ohmic voltage drop in molten salt (V)
E	cell potential during discharge (V)
E_{ocv}	cell e.m.f. (open circuit voltage) (V)
F	Faraday constant ($C\,mol^{-1}$)
I	current (cell current if not subscripted) (A)
$\bar{I}$	average current (A)
ΔI	transfer current (A)
$I_{o,a}$	exchange current at anode (A)
Δj	transfer current density ($A\,cm^{-3}$)
j_o	exchange current density in cathode ($A\,cm^{-3}$)
l	length (thickness) (cm)
n	amount of substance (mol)
n	number of electrons transferred per $FeCl_2$ (2)
R	resistance (Ω)
R'	non-ohmic electron transfer resistance (Ω)
R	gas constant ($J\,mol^{-1}\,K^{-1}$)
T	absolute temperature (K)
V	volume of cathode (cm^3)
v_i	volume of segment i in cathode (cm^3)
v_x	volume of solid phase x (cm^3)

Subscripts

e	effective
i	segment number, in cathode
j	time interval number
m	metal phase
s	molten salt phase
β	β''-alumina phase

Greek letters

α	parameter in Equation 9 (–)
ϵ	porosity (–)
η	overpotential (V)
η_a	anode overpotential (V)
η_c	cathode overpotential at β''-alumina interface (V)
κ	conductivity ($\Omega^{-1}\,cm^{-1}$)
ρ	resistivity ($\Omega\,cm$)

1. Introduction

Rechargeable sodium cells in which the cathode is a transition metal chloride have generated much research interest in recent years [1–22]. The most promising cathode materials are $FeCl_2$ and $NiCl_2$; for these cases, the overall cell reaction may be written as

$$2Na(l) + MCl_2(s) \rightleftharpoons M(s) + 2NaCl(s) \quad (1)$$

where M = Fe or Ni. The cathodes are fabricated in the discharged state by sintering a mixture of M and NaCl powders, a stoichiometric excess of the former being used in order to achieve adequate electronic conductivity in the fully charged cathode. A molten electrolyte of NaCl-saturated $AlCl_3$: NaCl floods the porous cathode, while β''-alumina solid electrolyte separates the anode and cathode compartments. Sodium ions migrate between anode and cathode during cell operation; the cathode reaction can thus be written as

$$MCl_2(s) + 2Na^+ + 2e^- \rightleftharpoons M(s) + 2NaCl(s) \quad (2)$$

A considerable amount of experimental data on the electrochemistry of these cells has already appeared, ranging from charge and discharge curves of full size cells (> 100 Ah) [4, 7, 15, 18] to the behaviour of small cathodes (~ 100 mAh) and simple wire electrodes in the molten electrolyte [11–13, 22].

The main anticipated application of sodium-metal chloride cells of the above type would be in batteries

* Author to whom correspondence should be addressed.

0021-891X

to power electric vehicles. Such cells would need to meet a variety of stringent performance criteria. Among these are the specific energy and the specific power, the latter quantity in a cell nearing full discharge being particularly important. These quantities are expected to depend critically on the details of cell and electrode design. Factors such as cell geometry (cylindrical with inner or outer cathode, or flat-plate), cathode thickness and cathode porosity will all have a major impact on cell performance.

Many full-sized cells have been built and tested with a view to investigating the effects of design parameters (2, 4, 7, 15–19]. This approach has drawbacks in that a thorough investigation of all the factors would involve very heavy investments of time and money. Furthermore, problems can arise with the reproducible fabrication of cells, increasing the uncertainty associated with experimental comparisons of cell performance.

Modelling of porous electrodes in electrochemical cells has been used to circumvent problems of the sort mentioned above [23–32]. Models can provide valuable insights into the parameters which are critical to the performance of a cell, and into the relative performance of cells with different design specifications. Some work has appeared on the modelling of sodium–metal chloride cells. Sudoh and Newman [29] have reported on a very detailed model while Nelson and coworkers [30–32] have published the results of calculations based on a simpler model. In this paper, we present a computer programmed model which combines a large degree of physical realism with relative simplicity and speed in use.

2. Previous models of sodium/metal chloride cells

Sudoh and Newman [29] have modelled the behaviour of sodium–iron chloride cells, where the performance of a porous iron chloride electrode (flooded with liquid electrolyte), a β''-alumina solid electrolyte separator and a liquid sodium anode are all taken into account. Modelling of the separator and anode are straightforward; the bulk of the modelling effort is devoted to the porous cathode. The analysis uses concentrated solution theory, and considers the mass transfer of the soluble ferrous complex in solution, to or from the metal, as well as the rate constant for precipitation and dissolution of the NaCl produced in the discharge process. Thus, although reagents and products are ultimately solids, the treatment implies a mechanism in which the electron transfer step involves solute species. Electron transfer kinetics are described by a suitable form of the Butler–Volmer equation.

Nelson and coworkers [30–32], have modelled the discharge behaviour of sodium–nickel chloride cells. In the most detailed description [30], the positive electrode is divided into 10 or 20 elements of equal volume, and the discharge process is divided into 100 equal time increments. The reaction current (transfer current) in each volume element at any state of charge is assumed to be proportional to the local overpotential and to the fraction of the original amount of $NiCl_2$ in the element which remains unreacted. The local transfer current is also inversely proportional to the reaction impedance, which is held constant throughout the entire discharge. The model has the advantage of being considerably simpler than that of Newman [29]; indeed, the necessary calculations were done by spreadsheet software on a personal computer. In contrast with the Newman model, Nelson's model does not allow for the solubility of NaCl or $NiCl_2$, nor does it use the full form of the Butler–Volmer equation.

The models described above are in principle capable of being compared with experimental data in various ways. In practice, there has been little effort in this direction, although Nelson's group have published plots of experimental and calculated area-specific impedances of the positive electrode against depth of discharge and found acceptable agreement over the range 0 to 90% discharge.

3. The present model

The present goal was to develop a model for sodium–iron chloride cells of different geometries which is realistic yet relatively simple, is reasonably easy to implement, is consistent with available experimental data and can be used to predict cell behaviour. Some degree of compromise is required between these requirements. Neither of the existing models was completely suitable for our purposes, nor are they in the public domain. It was therefore decided to proceed with the development of a new model. The focus of the investigation is on the performance of the cathode during discharge; design features such as dimensions of current collectors, liquid reservoirs, casings and other inactive areas of the cell are not considered.

3.1 *General description*

The model has been adapted to three different cell geometries, namely cylindrical cells with inner cathode, cylindrical cells with outer cathode, and flat-plate cells. We describe below the simpler flat-plate geometry shown in Fig. 1(a); the same principles apply to the cylindrical cells (Figs. 1(b) and (c)), with due allowance for the converging or diverging current paths.

The key features of the flat-plate cell are a solid planar current collector in contact with the three dimensional cathode, which in turn contacts a planar sheet of the β''-alumina solid electrolyte and the liquid sodium anode. The cathode consists of small particles of iron metal, iron chloride ($FeCl_2$) and salt (NaCl), in intimate contact. The pores within the solid mass are filled with the molten salt electrolyte, NaCl-saturated $AlCl_3$: NaCl. In a fully charged cathode, the only solids present are Fe and $FeCl_2$, and the porosity is at its maximum value. During discharge, Na^+ ions migrate from the anode, via the two electrolytes, to cathode sites

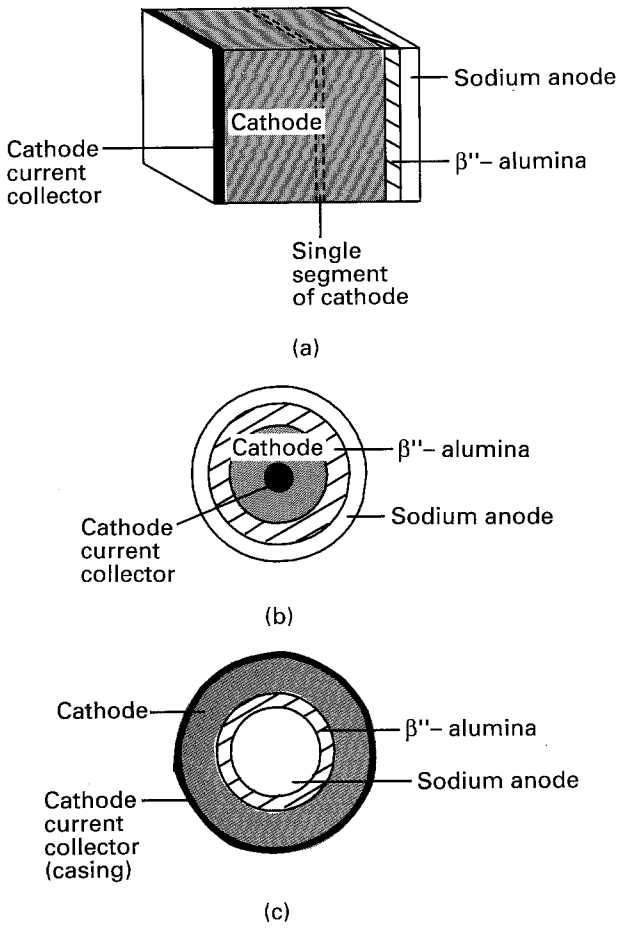

Fig. 1. Schematic cross-sections through cells: (a) flat-plate cell; (b) cylindrical cell, inner cathode; (c) cylindrical cell, outer cathode.

where Reaction 2 occurs. The pore volume decreases and some molten electrolyte flows out of the cathode; the cathode volume, i.e. the volume of solids plus pores, remains constant. A cathode (or region thereof) is completely discharged when no $FeCl_2$ remains.

Unlike the Newman model, the present model considers the cathode reaction to be effectively a solid state process. This approach is supported by some experimental results obtained at moderate temperatures (250° C) [11, 22]. Solubility of $FeCl_2$ and NaCl are thus not taken into account.

Current at the interface between the cathode and the β''-alumina is carried entirely by ions in the electrolyte. That is, $I_s = I$, where s represents the molten state electrolyte. At the current collector, the current is entirely electronic and is carried in the metal. At this point, $I_m = I$. Between these two extremes, current is transferred between electrolyte and metal phase. At any distance into the cathode, $I = I_s + I_m$. Ohm's law governs the potential within the electrolyte, and the electron transfer kinetics are described by a modified form of the Butler–Volmer equation, described more fully below.

On discharge, the cell potential, E, is equal to the open circuit voltage, E_{ocv}, minus the combined losses at the two electrodes and through the separator:

$$E = E_{ocv} - \eta_a - |\eta_c| - IR_\beta \tag{3}$$

where the overpotential, η, (and all other symbols in this paper) are cited in the initial listing.

3.2 *Segmentation of cathode*

For modelling purposes, the cathode is divided into a number (usually 100) of segments or laminae of equal thickness [24]. Current flow is perpendicular to the planes of the laminae. Within each segment, conditions are considered to be uniform (depth of discharge, overpotential, reaction rate, ionic current, electronic current).

The discharge process is also divided into equal time intervals, usually 0.01 h each. For each time interval, the overpotential, ionic current, voltage drop through the electrolyte and transfer current density (i.e. local reaction rate) is calculated for each segment. The instantaneous sum of the transfer currents ΔI_{ij} over all n segments must be equal in magnitude to the overall (fixed) current through the cell:

$$I = -\sum_{i=1}^{n} \Delta I_{ij} \tag{4}$$

The transfer current in a segment is related to the transfer current density by

$$\Delta I_{ij} = v_i \Delta j_{ij} \tag{5}$$

The minus sign in Equation 4 arises from the convention used in Equation 9 below, that cathodic currents are negative.

3.3 *State of charge*

Within segment i, after the jth time interval, a local depth of discharge d_{ij} can be defined as

$$d_{ij} = 1 - \frac{(n_{FeCl_2})_{ij}}{(n_{FeCl_2})_{i0}} \tag{6}$$

where the subscript 0 represents the fully charged state.

The instantaneous overall depth of discharge of the cathode, D_j can be calculated by suitable summation over all cathode segments:

$$D_j = \sum_{i=1}^{n} d_{ij} \frac{v_i}{V} \tag{7}$$

3.4 *Porosity of cathode*

At full charge or full discharge, the porosity (i.e. the volume fraction of molten salt) is uniform throughout the cathode. The instantaneous local porosity is given by

$$\epsilon_{ij} = 1 - \frac{(v_{Fe} + v_{FeCl_2} + v_{NaCl})_{ij}}{v_i} \tag{8}$$

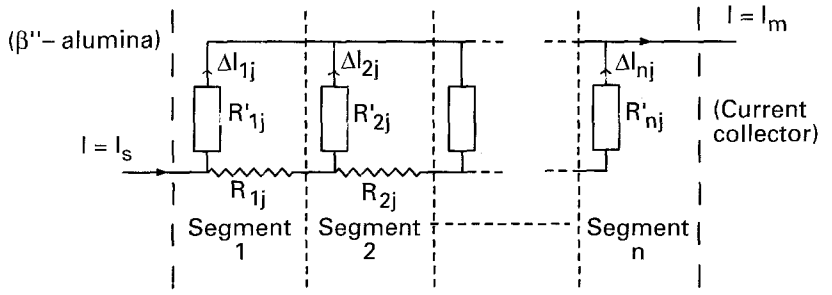

Fig. 2. Equivalent circuit of a porous cathode.

where the volumes of the various solids are calculated from their masses and bulk densities.

3.5 *Transfer current density in cathode*

The local, instantaneous transfer current density was calculated from the equation

$$\Delta j_{ij} = j_{0,ij}\left[\exp\left(\frac{(1-\alpha)n\eta_{ij}F}{RT}\right) - \exp\left(\frac{-\alpha n\eta_{ij}F}{RT}\right)\right] \tag{9}$$

where $j_{0,ij}$ is a local, instantaneous exchange current density. In one version of the model, this quantity is treated as a constant over the entire cathode and for all states of charge. This is somewhat unrealistic in that it implies that the discharge rate depends only on overpotential and not on the volume fraction of reagents remaining. More realistic discharge curves (see Section 4.1) are obtained if $j_{0,ij}$ is treated as being dependent on the instantaneous local state of charge. The two cases are represented by the equations

$$j_{0,ij} = j_0 \tag{10a}$$

and

$$j_{0,ij} = j_0(1 - d_{ij})^{2/3} \tag{10b}$$

The justification for the power of 2/3 employed in Equation 10b is that, for solid particles of regular shape, their interfacial area will vary as the two-thirds power of their volume. A cathode segment can be assigned a non-ohmic resistance to electron transfer, R'_{ij}, which corresponds to the current density–overpotential relationship of Equation 9 (see also Fig. 2).

3.6 *Anode kinetics*

The anode reaction on discharge is

$$\mathrm{Na}(l) \rightarrow \mathrm{Na}^+(\beta''\text{-alumina}) + \mathrm{e}^- \tag{11}$$

Provided that the β''-alumina is adequately wetted by the liquid sodium, this reaction should show excellent kinetics and the overpotential η_a at the anode is consequently very small. Thus the treatment of the anode kinetics is not at all critical as far as the overall performance of the cell is concerned. A linear current–potential relationship, as employed by Newman and Sudoh [29] was used:

$$I = \frac{I_{0,a}nF\eta_a}{RT} \tag{12}$$

3.7 *Ohmic losses*

Resistive voltage losses can, in principle, occur anywhere in the cell between the electrode terminals. The present model assumes that there are no ohmic losses between the anode terminal and the sodium/β''-alumina interface. Across the β''-alumina, the voltage loss is calculated as IR_β, where R_β is the resistance of the β''-alumina sheet, which is calculated from the resistivity in the usual way:

$$R_\beta = \frac{\rho_\beta l}{A} \tag{13}$$

where l is the thickness and A the area of the β''-alumina.

Within the cathode, resistive losses are particularly important. The model assumes that these losses are confined to the melt phase only, i.e. that the resistance of the metal matrix in the cathode is negligible compared with that of the molten salt. The effective, instantaneous, local conductivity of the melt phase, $\kappa_{e,ij}$, is related to its bulk conductivity κ and the local porosity of the cathode by the Bruggeman equation [33, 34]

$$\kappa_{e,ij} = \kappa\epsilon_{ij}^b \tag{14}$$

where $b = 1.5$ and is used to take into account the tortuosity of the current path through the melt. The resistance of an element of melt is then

$$R_{ij} = \frac{l_{ij}}{\kappa_{e,ij}A_{ij}} \tag{15}$$

and the ohmic voltage loss is

$$\Delta E_{ij} = \bar{I}_{s,ij}R_{ij} \tag{16}$$

where $\bar{I}_{s,ij}$ is the average current flowing through the molten electrolyte in segment i over time j (i.e. the average of the current flowing into the segment and the current flowing out of the segment). The local overpotential in the cathode varies as a direct result of the changing potential in the molten electrolyte, and is given by

$$\eta_{ij} = \eta_{(i-1)j} + \Delta E_{(i-1)j} \tag{17}$$

These overpotentials are by convention negative, while ΔE is positive. The overpotential η_{1j} in the first cathode segment (i.e. adjacent to the β''-alumina) is given by η_c.

3.8 *Temperature*

The model in its present state considers the operation of the cell to be isothermal. Parameters which would be expected to have significant temperature dependencies include exchange currents and the resistivities of the solid and liquid electrolytes. These can be allowed for in any given 'run', within the constraints of isothermal operation.

3.9 *Different cell geometries and operating conditions*

The model has been adapted to flat-plate cells and to cylindrical cells with both inner and outer cathodes. In principle, the behaviour of cathodes of any thickness and with any inner and outer radii can be simulated. The cathode porosity varies according to the ratio of NaCl to Fe in the discharged state, and can be varied at will. The discharge rate can be freely varied from one run to another.

3.10 *Program operation*

In the light of the foregoing description, the cathode can be represented by the equivalent circuit shown in Fig. 2. A trial value of η_c is selected, and the program then calculates the values of ΔI, I_s and η for each segment. Only one value of η_c will result in Equation 4 being satisfied, and successive approximations are used until this condition is met. The correct initial value of η_c has now been found. The amount of reaction occurring in each segment in the first time interval is calculated on the basis of this value of η_c, and the amounts of solid reagents and products present at the end of this interval are then calculated. For the second and subsequent time intervals, quantities such as the local exchange current and melt resistance will change, according to Equations 10b, 14 and 15. For each subsequent time interval the value of η_c is optimised by the successive approximation process. In this way the entire course of the cell discharge is calculated. At selected states of discharge relevant data such as cell voltage, distribution of reaction rate within the cathode and contributions to voltage losses are calculated and stored for subsequent retrieval and display.

4. Model calculations

4.1 *Fitting the model to experiment*

Values of many of the parameters needed in the program are available in the literature. Where possible, these have been used unchanged. While there have been measurements of exchange current densities at metal chloride electrodes of different types [11, 14, 21], there is a substantial spread in the results, according to the measurement procedure and physical form of the electrode. It was therefore decided to treat the exchange current density and transfer coefficient in Equation 9 purely as adjustable parameters. These quantities were chosen to obtain agreement between the calculated cell potential and selected experimental data at the beginning of the discharge. These two parameters were adjusted in tandem to obtain good fits to the two experimental discharge curves only at zero percent discharge. This fit is shown in Fig. 3, where the solid lines show calculated data for the model where the exchange current density in the cathode diminishes during discharge according to Equation 10b, while the dashed lines show the model predictions for a constant exchange current density, Equation 10a. No other adjustments were employed. Clearly the use of Equation 10a results in rather unrealistic discharge curves, in that the cell potential remains constant up to 60–70%, at which point the outer segments become fully discharged and the potential begins falling. In the remainder of the results reported here, Equation 10b was employed to describe the exchange current density. The experimental data for Fig. 3 were obtained from a cylindrical, internal cathode Na–$FeCl_2$ cell whose specifications are given in the caption [35].

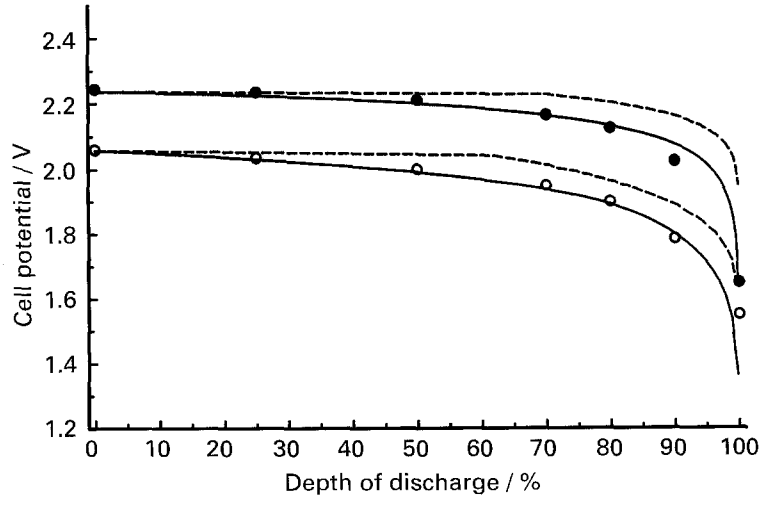

Fig. 3. Experimental and calculated discharge curves for a Na–$FeCl_2$ cell operating at 265° C (V_{OCV} = 2.345 V). (– – –), calculated using Equation 10a; (——), calculated using Equation 10b. Upper curves and experimental points (●): $C/2.5$ rate; lower curves and experimental points (○): $C/1$ rate. Cylindrical cell, inner cathode with outer radius 1.5 cm and thickness 0.35 cm. Cathode loading, 0.325 Ah g^{-1}(Fe) (i.e. 34% utilization of metal); cathode density, 0.327 Ah cm^{-3}; cathode height, 21 cm; β''-alumina thickness, 0.13 cm [35].

Table 1. Cell parameters used in the calculations

Geometry	flat-plate
Number of segments	100
Time increments	0.01 h
Metal utilization	34%
Capacity density	0.327 Ah cm^{-3}
Open circuit voltage	2.345 V
Operating temperature	265° C
Cathode exchange current density	0.12 A cm^{-3}
Anode exchange current density	5 A cm^{-2}
Transfer coefficient	0.2175
β''-Alumina thickness	0.085 cm
β''-Alumina resistivity	11 Ω cm at 265° C
Cathode thickness	varies
Discharge rate	varies

Values for the exchange current densities of the anode and cathode, the transfer coefficient, the resistivity of the β''-alumina, the number of segments and the length of time increments are given in Table 1.

Although there have been marked improvements in the fabrication of well-matched cells (an important requirement for cells to be incorporated into batteries), there is still some variability in the performance of full-size laboratory test cells. Thus the decision to fit the model to the experimental data of Fig. 3, rather than to any other set of data, is somewhat arbitrary, and the model as fitted would certainly not be expected to provide a good fit to all comparable cell data.

4.2 *Results*

Figures 4 to 9 below all refer to flat-plate cell geometry. Except where otherwise specified, the cell parameters for these Figures are as given in Table 1.

Figure 4 shows calculated discharge curves for flat-plate cells with cathodes of both 3 and 10 mm thickness, being discharged at various rates. The performance at high rates ($C/1$ to $C/2$) is particularly important for vehicle traction applications, where the poor performance of the thicker cathode is clearly evident. From a fuller set of such discharge curves it is possible to construct plots of cathode power density versus cathode thickness for specified discharge conditions. One such plot is shown in Fig. 5, which applies to cathode performance at 80% depth of discharge. There is only a slight fall-off in power density up to a cathode thickness of 5 mm, but thereafter the power density drops increasingly sharply as a result of the ohmic losses in the molten salt electrolyte.

With appropriate modifications, the present model is also capable of simulating the performance of cells with $NiCl_2$ cathodes. Comparisons have been made of calculated with experimental discharge curves for cylindrical, inner cathode cells of nominal 40 Ah capacity, discharging at various rates. Reasonable fits could be obtained at the lower rates ($C/4$ and $C/2$) but at higher rates ($C/1$ and $C/0.8$) the experimental curves do not curve downward as sharply at high degrees of discharge as do the calculated curves. Measurements have been made of the temperature rise occurring in cells during extended, fast discharge [36]. At the 1 h rate in a 40 Ah cell operating at a nominal temperature of 275° C, a temperature rise of ~ 85° C has been noted. This is expected to have a major effect on the electron transfer kinetics and on the electrolyte resistivities. In particular, the local overpotential in the cathode will be reduced through both the explicit temperature dependence of Equation 9 as well as the implicit temperature dependence of the exchange current density j_0. Since the model in its present form does not allow for temperature variation during a run, it is not expected to behave well under these circumstances. A model which considers heat generation and transfer within cells, and which allows for the temperature dependence of important cell parameters should therefore be a significant improvement when high discharge rates are involved.

Interesting insights into the operation of the cathode are obtained by studying the calculated transfer currents as a function of depth within the cathode. Examples are shown in Figs. 6 and 7. The reaction is much more evenly distributed over the thickness of the cathode in the thinner cathode (Fig. 6) than for the thicker cathode (Fig. 7). This phenomenon could be relevant to mechanisms of

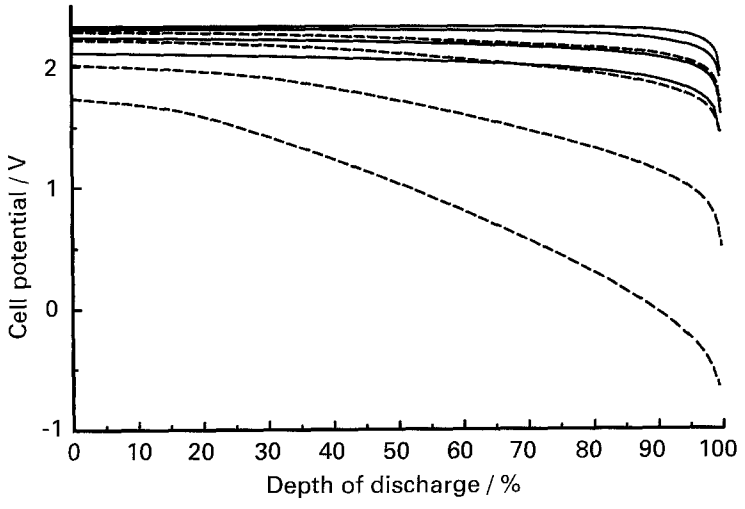

Fig. 4. Calculated discharge curves for flat-plate cell with 3 mm thick cathode (——) and 10 mm cathode (– – –). Rates (top to bottom in each set): $C/10$, $C/5$, $C/2$, $C/1$. Other cell details as in Table 1.

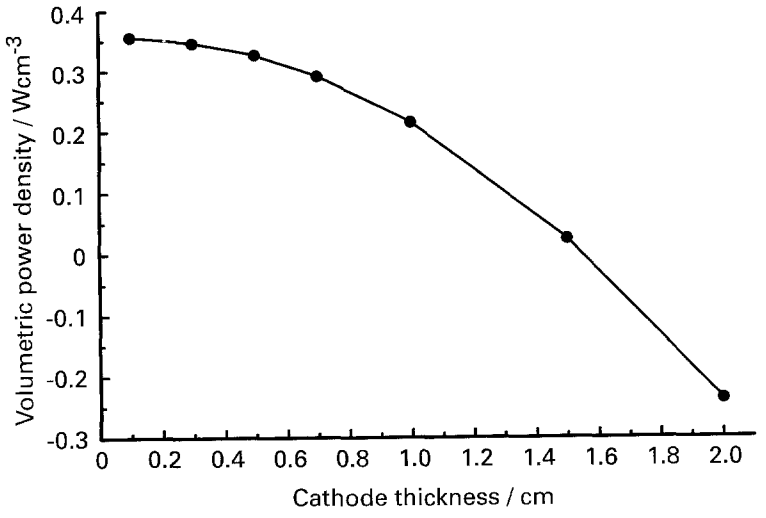

Fig. 5. Calculated cathode power density at 80% discharge versus cathode thickness. Flat-plate cell, $C/2$ rate, other details as in Table 1.

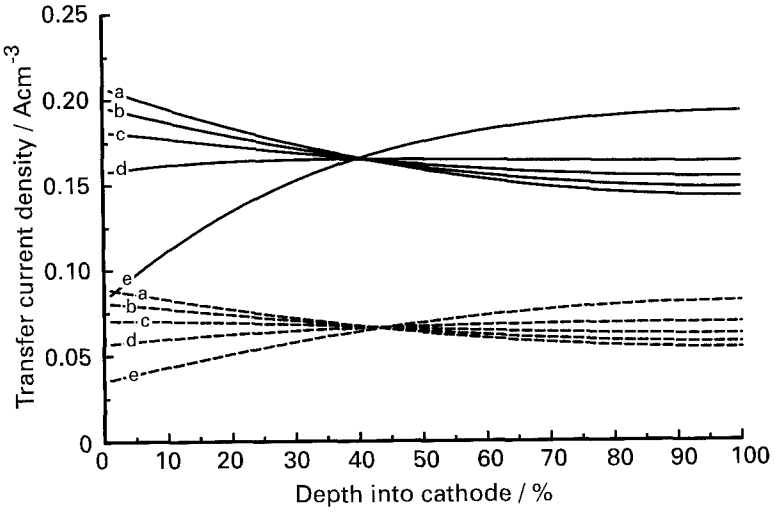

Fig. 6. Transfer current density versus depth into cathode for a planar 3 mm thick cathode at various states of discharge: (a) 10%, (b) 30%, (c) 50%, (d) 70% and (e) 90% discharged. (——), $C/2$ rate; (– – –), $C/5$ rate; other details as in Table 1.

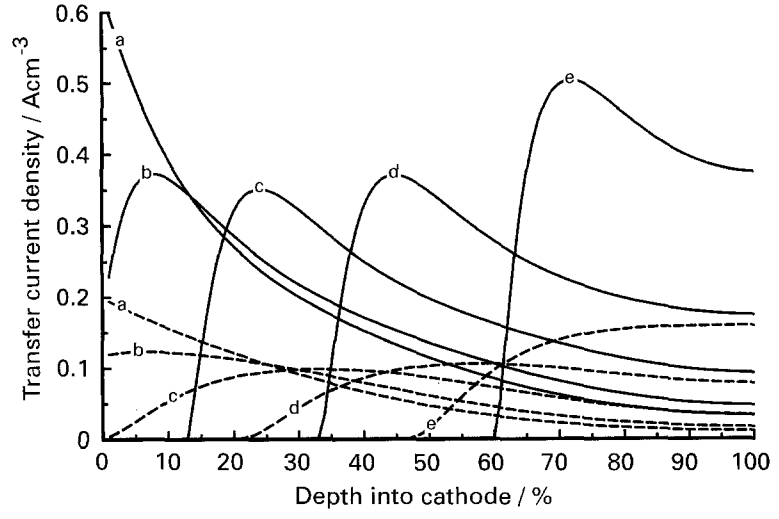

Fig. 7. Transfer current density versus depth into cathode for a planar 10 mm thick cathode at various states of discharge. Other details as for Fig. 6.

capacity loss in cathodes as a result of segregation of reagents. Higher discharge rates also lead to an increasingly skewed reaction rate distribution across the cathode; this is particularly evident with the thicker (10 mm) cathode of Fig. 7.

With the aid of the model it is also possible to analyse the individual contributions to internal power losses in the cell. These will depend on a number of factors, among which temperature, cathode porosity and the thicknesses of the cathode and the β''-alumina are particularly important. The anode kinetics are excellent and are never an important limitation to cell performance; in contrast, Fig. 8 shows that the cathode kinetics and the

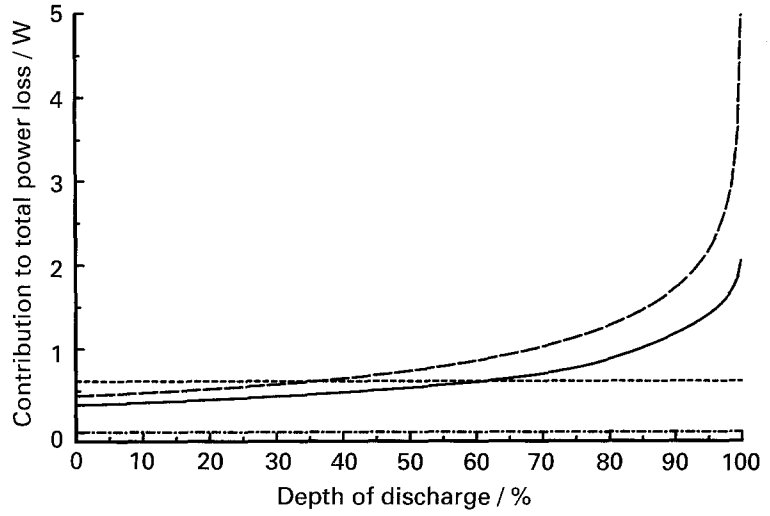

Fig. 8. Contributions to cathode power losses as a function of depth of discharge. Cell parameters as in Table 1. Cathode thickness, 0.5 cm; $C/2$ rate. Contribution from IR drop though β''-alumina (– – –); from IR drop through melt (——); from cathode overpotential (— —); from anode overpotential (–·–·–).

conductivities of both the solid and molten electrolytes are all important sources of electrical losses.

In the light of the above example, it is possible to conceive of improving cell performance through improvements in the main limiting parameters. These factors could in principle be modified by incorporating additives to the melt or the cathode solids, or by improvements in the electrical characteristics of the solid electrolyte. Figure 9 shows a 'standard' discharge curve as well as a set of hypothetical curves which would be anticipated if it were possible to double the conductivity of the β''-alumina, the conductivity of the melt and the exchange current density for the cathode reaction, respectively. Again it is evident that all of these factors are important, and that no great gains could be achieved through improvements in only one of them. In practice it appears unlikely that individual improvements as great as those considered above could easily be achieved.

Numerous other calculations can be, and have been, made using this program. The performances of cylindrical cells with inner and outer cathodes have been compared, and these have in turn been compared with flat-plate cells. The latter are obviously desirable from the point of efficient space utilization, though the thermal control of a multiple flat plate sandwich assembly would not be as easy as for a collection of cylindrical cells.

5. Discussion

The present model does not allow for dissolution, diffusion and reprecipitation of either NaCl or $FeCl_2$. These processes are expected to play an increasingly important role in the cathode chemistry as the operating temperature rises [22]. Related processes, such as the blocking of pores by precipitated salts and loss of capacity due to segregation of the cathode reagents are also beyond the scope of the model.

The model also ignores possible passivation of the cathode [11, 14], internal heat generation and dissipation in the cell, and the finite conductivity of the metallic 'backbone' in the cathode. Early experiments showed that it is necessary to use a substantial excess of metal over the stoichiometric amount required by Reactions 1 or 2 [5]. Insufficient metal leads to lowered capacity, apparently due to inactive regions in the cathode arising from discontinuities in the electron-conducting network. The model incorporates the use of excess metal (only 34% of the metal is

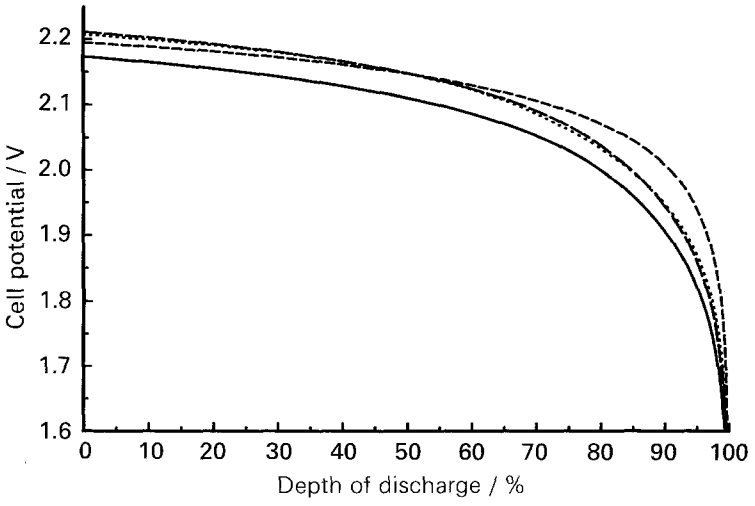

Fig. 9. Effect on discharge curves of hypothetical improvement in selected parameters. Cathode thickness, 0.5 cm; $C/2$ rate. Predicted performance with other parameters as given in Table 1 (——); effects of doubling conductivity of β''-alumina (— —); doubling melt conductivity (– – –); doubling exchange current density of cathode reaction (·····). (Doubling the anode exchange current density has a negligible effect).

actively utilised in the examples provided in this paper), but is incapable of simulating the effects of insufficient metal on the cathode capacity.

Some of the above limitations could be addressed by more sophisticated models, at the expense of increased program complexity and longer running times. Indeed, the model proposed by Sudoh and Newman does consider salt solubilities, but requires the introduction of somewhat arbitrary parameters to describe the dissolution and precipitation rates [29].

The model is capable of achieving a good fit to experimental data without resorting to an undue number of adjustable parameters. Application of the model has provided some useful insights into the cell performance in general and the detailed operation of the cathode in particular. For example, the calculations of Fig. 9 suggest that substantial improvements in cell performance will not be achieved by concentrating on any single factor; electrolyte resistivities and cathode kinetics are all significant limitations to performance at present.

Acknowledgements

We thank the University of the Witwatersrand and the Foundation for Research Development for financial support.

References

[1] J. Coetzer, *J. Power Sources* **18** (1986) 377.
[2] R. J. Bones, D. A. Teagle, S. D. Brooker, F. L. Cullen and J. Lumsdon, *Proc. Electrochem. Soc.* **87–12** (Proc. 2nd Symp. Electrode Mater. Processes Energy Convers. Storage), (1987) 537.
[3] R. C. Galloway, *J. Electrochem. Soc.* **134** (1987) 256.
[4] R. J. Bones, J. Coetzer, R. C. Galloway and D. A. Teagle, *ibid.* **134** (1987) 2379.
[5] J. L. Sudworth, *Chemistry and Industry* (1988) 77.
[6] K. T. Adendorff and M. M. Thackeray, *J. Electrochem. Soc.* **135** (1988) 2121.
[7] R. J. Bones, D. A. Teagle, S. D. Brooker and F. L. Cullen, *ibid.* **136** (1989) 1274.
[8] P. T. Mosley, R. J. Bones, D. A. Teagle, B. A. Bellamy and R. W. M. Hawes, *ibid.* **136** (1989) 1361.
[9] L. Redey and D. R. Vissers, The Electrochemical Society Meeting, Hollywood, FL, (October 1989) *Ext. Abstr.* **89–2** Abstr. 95, 143.
[10] I. Bloom, S. K. Orth and D. R. Vissers, The Electrochemical Society Meeting, Hollywood, FL, (October 1989), *Ext. Abstr.* **89–2** Abstr. 96, 145.
[11] B. V. Ratnakumar, S. Di Stefano and G. Halpert, *J. Electrochem. Soc.* **137** (1990) 2991.
[12] S. W. Orchard and G. Mamantov, *ibid.* **136** (1989) 3565.
[13] J. S. Weaving and S. W. Orchard, *J. Power Sources* **36** (1991) 537.
[14] B. V. Ratnakumar, A. I. Attia and G. Halpert, *ibid.* **36** (1991) 385.
[15] R. J. Bones, D. A. Teagle and S. D. Brooker, Proc. 16th Int. Power Sources Symp., Bournemouth (September 1988) p. 537.
[16] N. D. Nicholson, D. S. Demott and R. Hutchings, *ibid.*, p. 549.
[17] R. J. Wedlake, J. Coetzer and I. L. Vlok, *ibid.*, p. 563.
[18] R. M. Dell and R. J. Bones, Proc. 22nd Intersoc. Energy Convers. Eng. Conf. (Vol. 2), (1987) p. 1072.
[19] A. R. Tilley and R. N. Bull, *ibid.*, p. 1078.
[20] R. J. Wedlake and A. R. Tilley, *B. Electrochem.* **4** (1988) 41.
[21] B. V. Ratnakumar, S. Di Stefano and C. P. Bankston, Proc. 24th Intersoc. Energy Convers. Eng. Conf. (Vol. 6), (1989) p. 2921.
[22] J. Coetzer, G. D. Wald and S. W. Orchard, *J. Appl. Electrochem.*, in press.
[23] J. Newman and W. Tiedemann, *AIChE Journal* **21** (1975) 25.
[24] J. Euler and W. Nonnenmacher, *Electrochim. Acta* **2** (1960) 268.
[25] J. S. Newman and C. W. Tobias, *J. Electrochem. Soc.* **109** (1962) 1183.
[26] E. A. Grens II and C. W. Tobias, *Electrochim. Acta* **10** (1965) 761.
[27] E. A. Grens II and C. W. Tobias, *Ber. Bunsenges. Phys. Chem.* **68** (1964) 236.
[28] R. De Levie, *in* 'Advances in Electrochemistry and Electrochemical Engineering', Vol. 6, (edited by P. Delahay), John Wiley & Sons, New York (1967) p. 329.
[29] M. Sudoh and J. Newman, *J. Electrochem. Soc.*, **137** (1990) 876.
[30] I. Bloom, P. A. Nelson, L. Redey, S. K. Orth, C. L. Hammer, R. S. Skocypec, D. W. Dees, M. C. Hash and D. R. Vissers, Proc 25th Intersoc. Energy Convers. Eng. Conf. (Vol. 3), (1990) p. 341.
[31] P. A. Nelson and J. Prakash, *Proc. Electrochem. Soc.* **91–10** (Proc. Symp. Model. Batteries Fuel Cells), (1991) p. 122.
[32] P. A. Nelson, Proc. 24th Intersoc. Energy Convers. Eng. Conf. (Vol. 3), (1989) p. 1363.
[33] F. M. Delnick and R. A. Guidotti, *J. Electrochem. Soc.* **137** (1990) 11.
[34] D. A. G. Bruggeman, *Ann. Phys.* **24** (1935) 636.
[35] Experimental data kindly provided by I. L. Vlok, Zebra Power Systems.
[36] J. L. Sudworth and R. N. Bull, Presented at EPRI and US DOE Beta Battery Workshop VII (June 1988).